A CONSERVATIVE ZONAL APPROACH WITH APPLICATIONS TO UNSTEADY TURBOMACHINERY FLOWS

Hong Yang, Dirk Nürnburger and Anton Weber
Institute of Propulsion Technology, DLR
Linder Höhe, 51147 Köln

1. INTRODUCTION

A conservative and accurate interfacing algorithm would be very important to both structured and unstructured Navier-Stokes solvers for tackling sliding-grid problem, which is often encountered in turbomachinery if considering the interaction between rotating and non-rotating components. Furthermore, application of structured CFD solver to complex geometries is often hindered by huge manpower consumed on generating block-structured grid with only 1-to-1 matched block interfaces. Hence, a mismatched grid interface would be very necessary not only to the sliding grids, but also to ease of block-structured grid generation. To solve the mismatched interface problem, a multi-zonal approach needs to be developed as conservatively and accurately as possible .

There are two categories of multi-zonal approaches in the literature, namely, overlapped (Chimera) grid approach and patched (zonal) grid approach. The patched grid approach, which is simply called as zonal approach in this paper, shows an attractive advantage over the Chimera method on conservation due to with only one shared boundary between two patched zones, such that it is much easier to maintain conservation . A systematic study on the cell-vertex based (finite difference) patched grid approach was carried by Rai [1], who proposed a conservative zonal scheme firstly for 2-D Euler equations, and latter applied it to 3-D Navier-Stokes equations. The main idea of the Rai's scheme is to retain conservation by interpolating fluxes at the interface for only one of two patched zones, while to ensure continuity by interpolating dependent variables at the interface for the other zone. However, in the Rai's scheme, the fluxes are evaluated by the finite difference method, and therefore, the flux conservation across the zonal boundaries is not entirely satisfied. One application of the Rai's scheme was performed by Hessinius and Rai in the 3-D Euler computations on wing-canard combination [2]. But their implementation requires the zonal interface be planar, one of common restrictions in most implementations of this technique due to the minor gaps and overlaps that occur at a curved interface if the two zones are not mesh continuous. Similar to the Rai's scheme, Walters et al. also implemented the patched grid scheme in their 2-D/3-D Euler solver with the MUSCL upwind scheme [3]. Additionally, to solve the problem of curved interface, Furukawa et al. [4] and Klopfer et al. [5] proposed special approaches to ensure uniqueness of zonal boundary. However, their uniqueness methods are too hard to be generalized or to be extended to 3-D computations.

In this paper, we present a fully conservative and second-order-accurate zonal approach that allows zonal interface to be stationary/sliding and planar/curved. This zonal approach has been incorporated into the state-of-the-art unsteady/steady Navier-Stokes solver *TRACE* at the DLR. It is dedicated to the multi-zonal/block structured grids with so called "unstructured block-cuts" at the patched boundaries. The zonal approach is intended to solve all types of known interfacing problems within turbomachines, and so far has been validated by a variety of testcases, including both axial and radial compressors as well as turbines, especially on the topics of stator-rotor interaction, casing treatment, and sealing air injection cavity. This paper will present some validation results and applications to the study of unsteadyness and clocking effect due to stator-rotor interaction in a one and half stage turbine.

2. NUMERICAL ALGORITHM

The unsteady/steady Navier-Stokes solver *TRACE* is being applied by a growing user community both in research and industry. In this solver, under the relative frame of reference, the 3-D Reynolds-averaged Navier-Stokes equations are integrated in time by a fully implicit formulation of the second-order scheme for the compressible ideal gas in conjunction with the Spalart-Allmaras turbulence model. The convective fluxes are discretized using Roe's TVD upwind scheme which is combined with van Leer's MUSCL extrapolation to obtain second-order accuracy in space. The derivatives of the viscous fluxes are approximated by central diferences.

Consistent with the numerical schemes on the interior cells, the same Roe's upwind and central differencing formulations are applied to evaluate the convective fluxes and the viscous fluxes, respectively at only one side of the zonal interface shared by two patched zones, while for the other side of the zonal interface, a conservative rezoning has to be performed based on the known fluxes from its partner side and the grid overlapping relation at the zonal interface. Hence, the zonal approach can be divided into two stages, namely, flux construction and flux conservation as follows.

2.1 Flux Construction

At the mismatched zonal interafce or so called "unstructured block-cut" $j_{1m}+1/2$ shown in Fig.1, the total numerical flux vector $(\hat{F}_t)_{j_{1m}+1/2}$ is calculated as follows

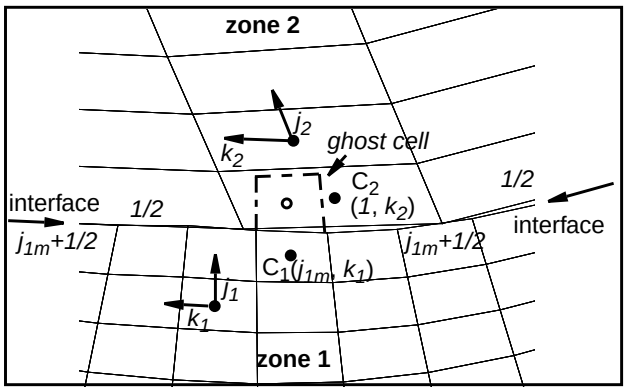

Fig. 1 Mismatched interface between two patched grids (the 3rd index nomal to paper "*l*" is neglected)

$$(1)\qquad (\hat{F}_t)_{j_{1m}+1/2} = (\hat{F}_c)_{j_{1m}+1/2} - \frac{1}{Re_0}(\hat{F}_v)_{j_{1m}+1/2}$$

where $(\hat{F}_c)_{j_{1m}+1/2}$ and $(\hat{F}_v)_{j_{1m}+1/2}$ are convective and viscous flux vectors, respectively. The convective flux vector is calculated with the Roe's upwind scheme [6], while the viscous flux vector is discretized by the central differencing scheme, and Re_0 is reference Reynolds number. If the MUSCL-type approach of the 2nd-order-accurate upwind scheme is applied at boundary cells, usually two layers of ghost cells are needed to calculate the right or left states at the boundary face. However, at the zonal interface boundary, for instance, concerning zone *1* in Fig. 1, if the right states are interpolated from zone *2*, only one layer of ghost cells is needed to evaluate the left states at face j_{1m}*+1/2*. Therefore in our zonal approach, only one layer of ghost cells beside the zonal interface is necessarily created for both patched zones by a simple extrapolation from the interior cells, and the conserved variables at the ghost cells are interpolated from those of the zonal cells* pertaining to the partner side, such that, the left states of face j_{1m}*+1/2* in zone *1,* and right states of face j_2*=1/2* in zone *2* can be MUSCL extrapolated. Then the right states of face j_{1m}*+1/2* can be interpolated from the right states of face j_2*=1/2* in zone *2* . With the correct left and right states, the convective fluxes at face j_{1m}*+1/2* can be calculated via Roe's approximate Riemann solver [6]. Finally, the total fluxes at face j_{1m}*+1/2* can be evaluated with Eq. (1) after the viscous fluxes being calculated with the central differencing scheme.

2.2 Flux Conservation

To have conservation across zonal interface boundary, the numerical fluxes at zonal interface j_2*=1/2* in zone *2* must be calculated with a conservative **rezoning**[7] algorithm based on the known fluxes over the face j_{1m}*+1/2*:

$$(2)\ (\hat{F}_t)_{1/2,k_2,l_2} = \sum_{k_1^\dagger l_1^\dagger} \sum (\hat{F}_t)_{j_{1m}+1/2,k_1^\dagger,l_1^\dagger} \frac{(\Delta S)^{1/2,k_2,l_2}_{j_{1m}+1/2,k_1^\dagger,l_1^\dagger}}{S_{j_{1m}+1/2,k_1^\dagger,l_1^\dagger}}$$

where $S_{j_{1m}+1/2,k_1^\dagger,l_1^\dagger}$ is the face area of the zonal cells of zone *1* which overlap the cell face $(1/2, k_2, l_2)$ of zone *2*; $(\Delta S)^{1/2,k_2,l_2}_{j_{1m}+1/2,k_1^\dagger,l_1^\dagger}$ is the overlapped area between the cell face $(1/2, k_2, l_2)$ and the cell face $(j_{1m}+1/2, k_1^\dagger, l_1^\dagger)$; and $k_1^\dagger$, $l_1^\dagger$ denote relative indices of zonal cell faces in zone *1* which overlap with the cell interface $(1/2, k_2, l_2)$ pertaining to zone *2*. Eq. (2) is derived by assuming the fluxes are piecewise constant within a cell face at the zonal boundary.

To handle the curved zonal interface, a generalized geometry interfacing algorithm is developed in the local coordinates system, and therefore all interfacing work has to be done under the local coordinates system. The overlapped area ΔS in Eq. (2) is calculated by the "clipping algorithm†" borrowed from the computer graphics field [8] with appropriate modification. For two patched grids, at the zonal interface, one grid that supplies the fluxes is called as donor grid, while the other one on which the rezoning is required is called as recipient grid. Due to the gap and clearance existed at curved zonal interface, the overlapped area should be calculated from the donor grid side in order to make flux conservation across the zonal interface so that the recipient grid be used to clip the donor grid at the zonal interface. Actually in this way, we can achieve the effect of uniqueness of patched zonal boundaries. Furthermore, at zonal interface boundary, bilinear interpolation is applied for all necessary interpolation calculations in the zonal approach. To make the zonal approach fast and robust, a sophisticated search algorithm is developed on the basis of computational geometry and isoparametric mapping technique [9]. Regarding the flux conservation across the zonal interface, one should notice that flux transformation from one frame of reference to the other may be necessary if two adjoining zones are in different frames of reference. Therefore, if rezoning calculation is performed in the absolute frame of reference, then for the recipient grid the rezoning fluxes at *LHS* of Eq. (2) need to be transformed to the appropriate frame of reference under which the recipient domain is discretized. In addition, this zonal approach has been parallelized as well with the help of MPI / PVM communication libraries. An asymmetric communication routine has been taken for sending and receiving data between two patched zones.

3. VALIDATION

The zonal approach has been validated by a variety of tetscases with respect to turbomachinery. In this paper, we only present validation results for two testcases, one with stationary and the other with sliding zonal interfaces.

3.1 Testcase 1 - Stationary Zoanl Interface

This testcsase is about a single turbine rotor typically with large camber curvature that often brings about difficulties

*. interior cells adjacent to the zonal boundary

†. to remove that part of image (a polygon) that falls outside of the boundary of a graphics window.

to the structured grid generation in the tip clearance. Fig.2 shows two grids are generated in the tip clearance, one is with unstructured bock-cut (curved zonal interface), and the other only with structured block-cut. The steady flow through this rotor has been simulated with both grid topologies in Fig. 2 for the sake of comparison. The calculated massflow rates at entry and exit boundaries have shown that a converged and conserved solution can be reached with the zonal approach, due to that the relative massflow error between entry and exit boundaries is less than 0.0001% after 2000 time steps. Fig. 3 gives the convergence history, from which one can find that the zonal approach has resulted into a similar convergent performance to the one on the grid with only structured block-cut, and Fig. 2 (c) illustrates nearly the same pressure distribution has been obtained in the tip clearance with different grid topologies. Fig. 4 compares the radial distribution of circumferentially averaged Mach number at a measuring plane after the rotor blades. Although in the experiment, there is an additional blade row downstream of the rotor blade row, one can still find a fairly good agreement between the predicted and experimental data in Fig. 4.

3.2 Testcase 2 - Sliding Zonal Interface

The unsteady flow through a 1.5-stage Aachen rig turbine [10], corresponding to so called “BIG” massflow, is simulated with the zonal approach. To retrive the space and time flow periodicity on a minimum number of blade passages, two stator blade rows are scaled in terms of blade count and profile to yield identical pitch distances on both sides of each rotor/stator zonal interface and to keep loadings on stators unchanged with the same picth-chord ratio as original. Quite coarse grid, i.e., 342,726 mesh cells (49 points in radial direction) is used to discretize the computational domain. Fig. 5 shows the block-structured grid, mismatched zonal interface and two measureing planes for this testcase. Within every rotor passing period, 128 time steps are calculated, each of which contains 20 subiterations for the dual time stepping. Figs. 6 and 7 present the convergence history for instantaneous and time-averaged isentropic efficiency respectively, from which one can find that after about 15 rotor passing periods, full time periodicity, or equivalently, the convergent state is reached. Figs. 9 and 10 compare the time-averaged Mach number distributions between the experiment and the prediction at axial planes 2 and 3 that locate before and after stator 2, respectively. At axial plane 2, one can find the affected area of rotor passage and trailing edge vortices, and additionally the tip clearance vortex by the calculation, while at axial plane 3, the wake and passage vortices of stator 2 together with the rotor passage vortices are also discernible in the predicted result. Recall the difference of geometry and blade counts between the prediction and the experiment, and the coarse grid used in the calculation, the predicted results may be regarded as being qualitatively in agreement with the measurement. Fig. 11 shows unsteady (instantaneous minus time-mean) pressure and unsteady velocity vector acting on stator 2 within one rotor passing period *T*. In Fig. 11, TI is time index, and TI= *1*, *17*, *33*, *49* correspond to *0*, *T/4*, *T/2*, *3T/4*, respectively. From Fig. 11, one can see clearly the time-dependent unsteadyness on the stator 2 blade row due to the wakes from upstream blade rows, which may explain the pressure perturbations within stator 2 arise largely as a result of recirculating unsteady velocity field that is established within stator 2 blade passage. Finally, Figs. 12 and 13 compare instantaneous unsteadyness in terms of unsteady kinetic energy between experiment and prediction at axial planes 2 and 3, respectively. These two figures convince us that the unsteadyness due to stator/rotor interaction can be predicted fairly well with the help of our zonal approach.

4. APPLICATION - CLOCKING EFFECT

The clocking effect of stators in testcase 2 is numerically analyzed as an application of the zonal approach. Five clocking angles, i.e., 0, 2, 4, 6, and 8 degree, are considered here, and the clocking direction of stator 2 is shown in Fig. 5. The calculated time-averaged isentropic efficiency for the 1.5 stage and the total pressure loss coefficient for stator 2 are given by Fig. 8, in which one can find the highest and lowest efficiencies correspond to clocking angles of 2 (deg.) and 6 (deg.), respectively, and their relative difference is 0.23% (total pressure loss difference: 2.58%). The instantaneous entropy distribution in Fig. 14 and the FFT harmonics of pressure on stator 2 blade surfaces in Fig. 15 can help us to understand the clocking effect. For clocking angle of 6 deg., the wakes from stator 1 and partial wakes of rotor blades reach the middle of stator 2 blade passage and then mix with the mainflow of stator 2; whereas for clocking angle of 2 deg., the stator 1 wake impinges upon stator 2 blade leading edge, and afterwards its core moves along the blade pressure surface while the core of rotor wake only migrates aorund the suction surface after being chopped by the stator 2 blade, resulting in the least disturbance to the mainflow in stator 2 blade passage.

5. CONCLUDING REMARKS

A conservative and second-order-accurate zonal approach has been developed with consistent differencing schemes as those applied at interior cell faces. Flux conservation is ensured by evaluating the fluxes at one side of the zonal interface which is latter used in the conservative rezoning calculation at the other side; while the continuity is achieved by the interpolation of states at the zonal interface. Two testcases with stationary curved and sliding planar zonal iterfaces have validated the zonal approach in terms of conservation, accuracy and robustness. As an application, the clocking effect of two stators in a 1.5 stage turbine has been numerically simulated and an optimal clocking angle is thus figured out. Further applications of this zonal approach will be published in the future.

6. REFERENCES

[1] Rai M.M., A Conservative Treatment of Zonal Boundaries for Euler Equation Calculations, AIAA 84-0164
[2] Hessenius K.A., Rai M.M., Three-Dimensional Conservative, Euler, Computations Using Patched Grid Systems and Explicit Methods, AIAA 86-1081, 1986
[3] Walters R.W., et al., Aspect and Applications of Patched Grid Calculations, AIAA 86-1063, 1986
[4] Furukawa M., et al., A Zonal Approach for Solving the Compressible Navier-Stokes Equations Using a TVD Finite Volume Method, JSME Int. J., Series II, Vol. 33, pp.665-673, 1990
[5] Klopfer G.H. et al., Conservative Multizonal Interface Algorithm for the 3-D Navier-Stokes Equations, AIAA-91-1601-CP, 1991
[6] Roe P.L., Approximate Riemann Solvers, Parameter Ve-

ctors and Difference Schemes, J. Comp. Phys., Vol. 43, pp.357-372, 1981
[7] Ramshaw J.D., Conservative Rezoning Algorithm for Generalized Two-Dimensional Meshes", J. Comp. Phys., Vol. 59, pp.193, 1985
[8] Newmann W.M., et al., Principles of Interactive Computer Graphics, McGraw-Hill, New York, pp.69-72, 1979
[9] Ergratoudis I., et al., Curved, Isoparametric, Quadrilateral Elements for Finte Element Analysis, Int. J. Solid Structure, Vol. 4, pp.31-42, 1968
[10] Walraevens R.E., Stephan B., Testcase U1 - 1-1/2 Stage Flow Turbine, ERCOFTAC SIG on 3D Turbomachinery Flow Predicition, RWTH Aachen, 1998

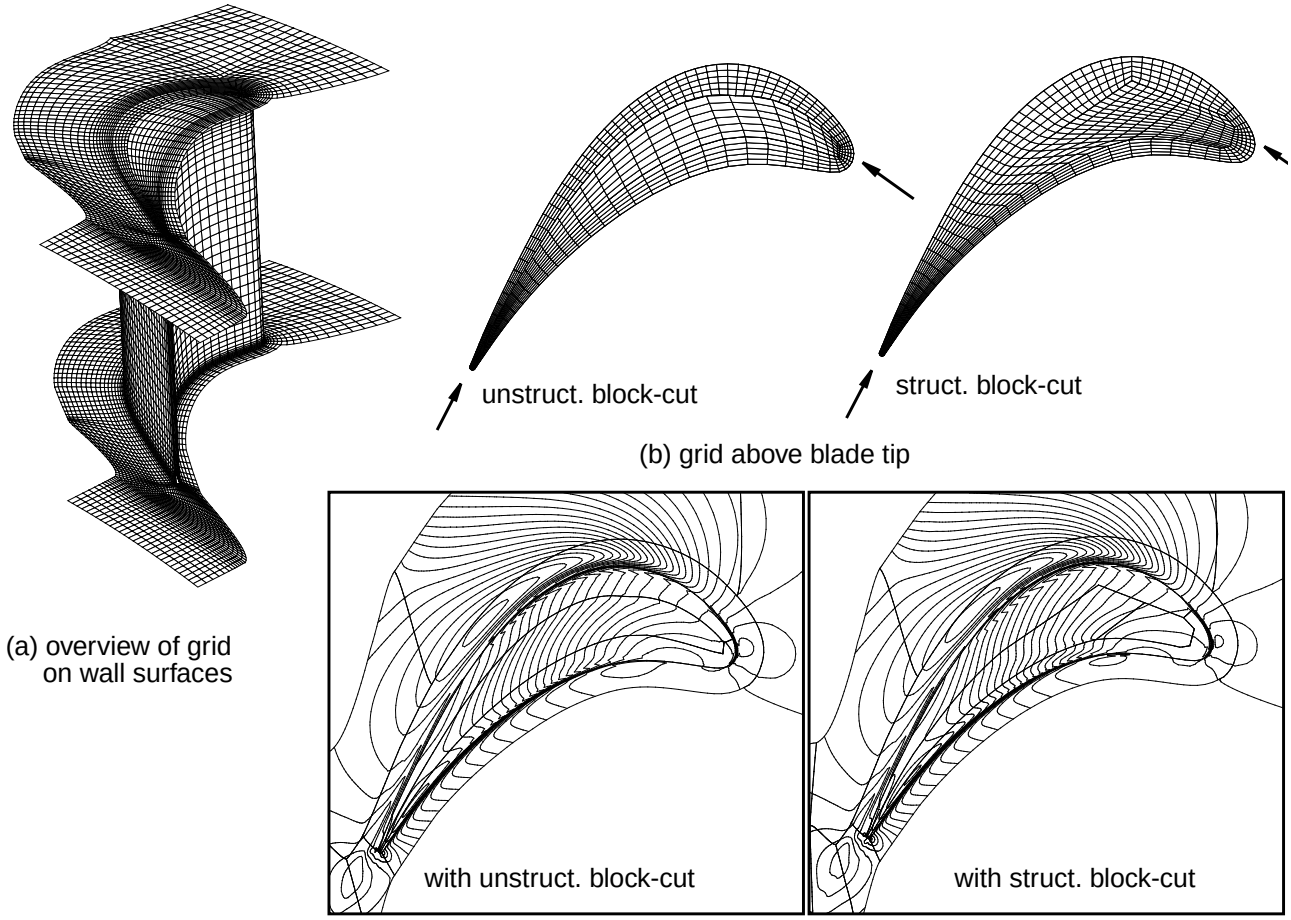

(a) overview of grid on wall surfaces

(b) grid above blade tip

(c) Calculated pressure contours in the middle of tip clearance

Fig. 2 Application to stationary zonal interface in tip clearance of a turbine rotor

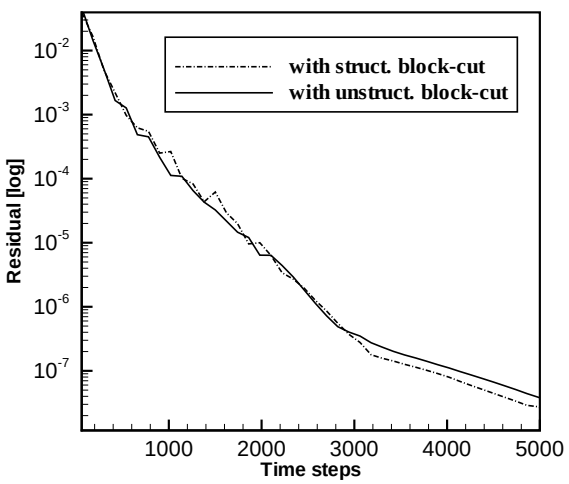

Fig.3 Residual history for the rotor testcase

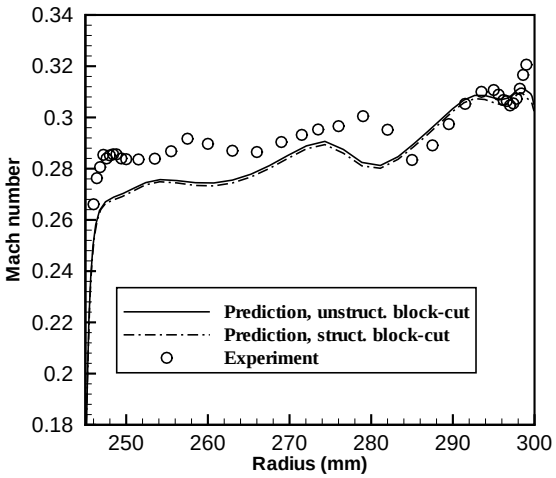

Fig. 4 Radial distribution of circumferentially-averaged Mach number at rotor exit

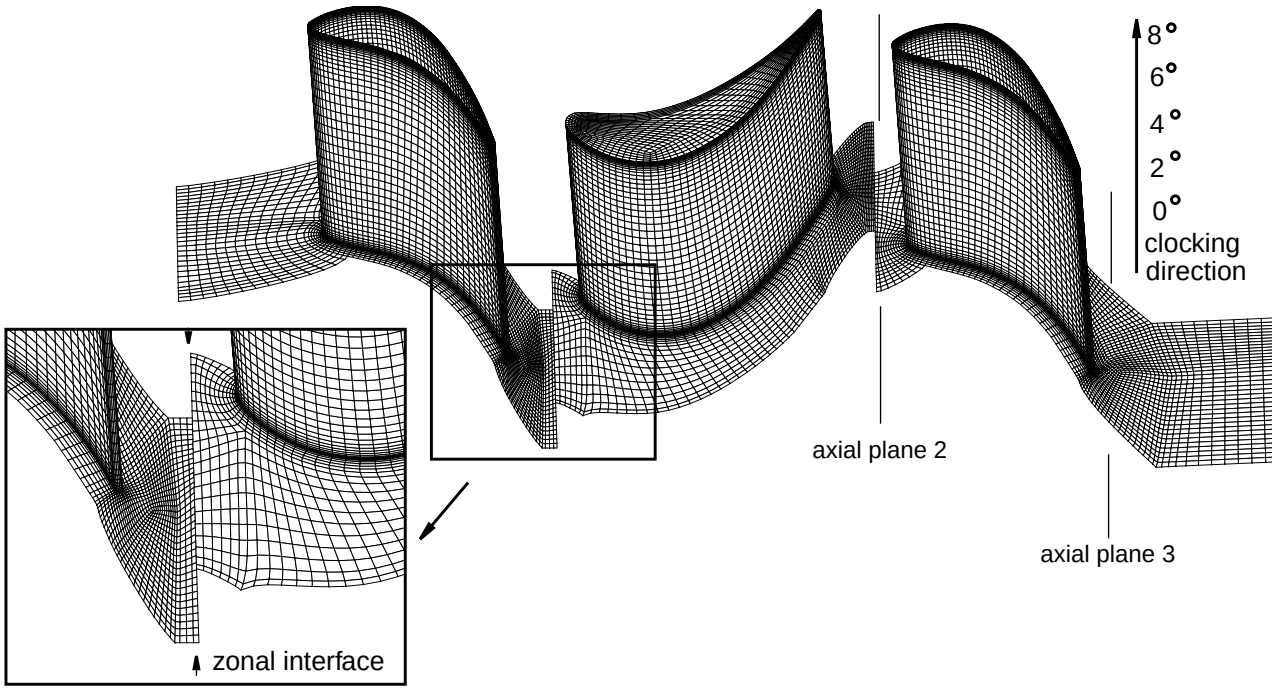

Fig. 5 Grids for one and half stage turbine testcase with notation of clocking direction

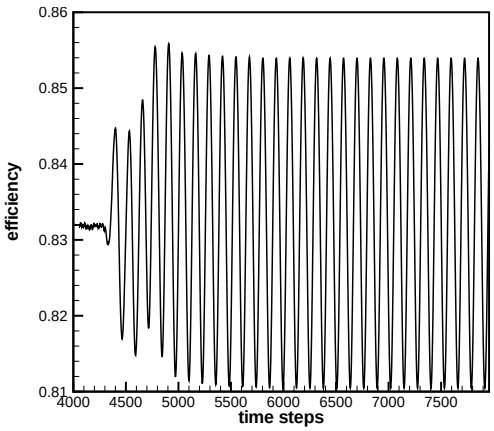

Fig. 6 Isentropic efficiency vs. timesteps

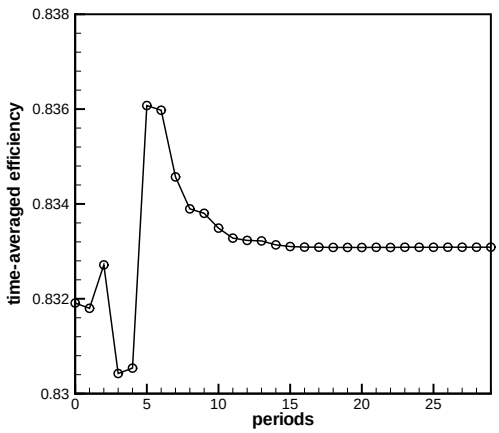

Fig. 7 Time-averaged isentropic efficiency vs. rotor passing periods

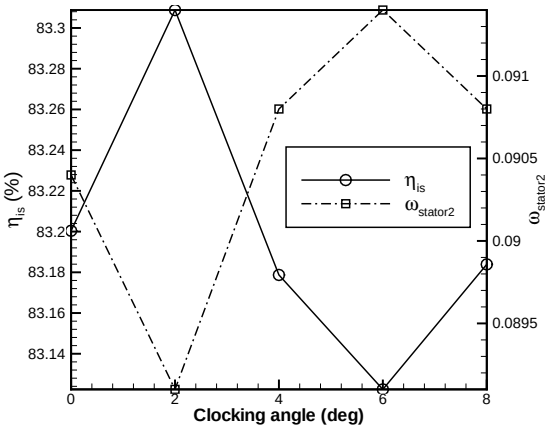

Fig. 8 Effect of clocking angles on time-averaged efficiency of 1.5-stage turbine and on time-averaged total pressure loss coefficient in stator 2

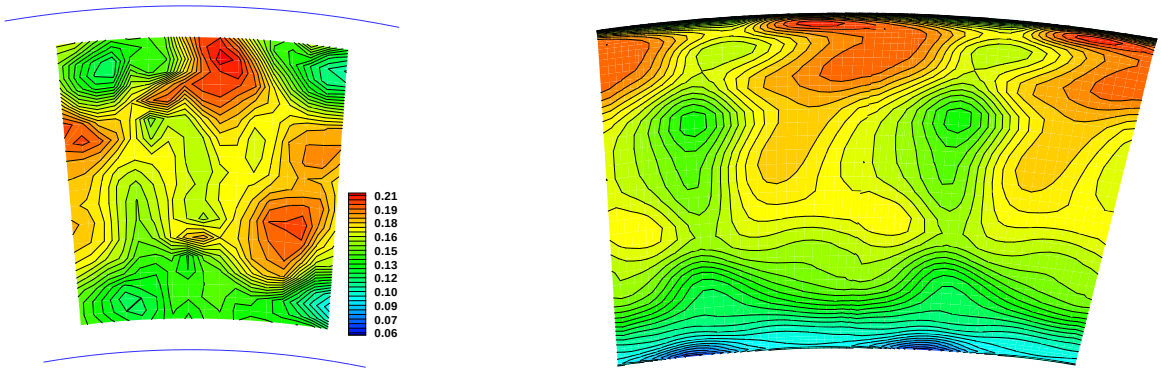

(a) measurement (1.2 pitch) (b) predicition (2 pitches)

Fig. 9 Time-averaged Mach number contours at axial plane 2

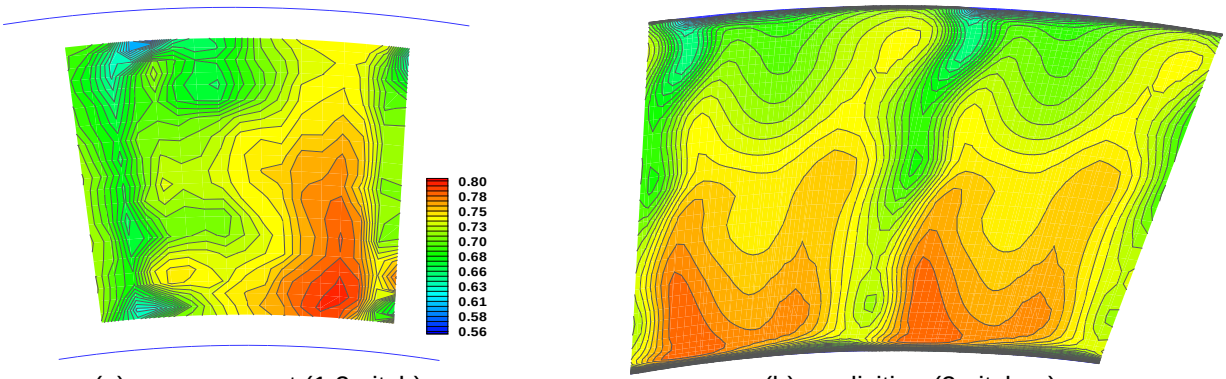

(a) measurement (1.2 pitch) (b) predicition (2 pitches)

Fig. 10 Time-averaged Mach number contours at axial plane 3

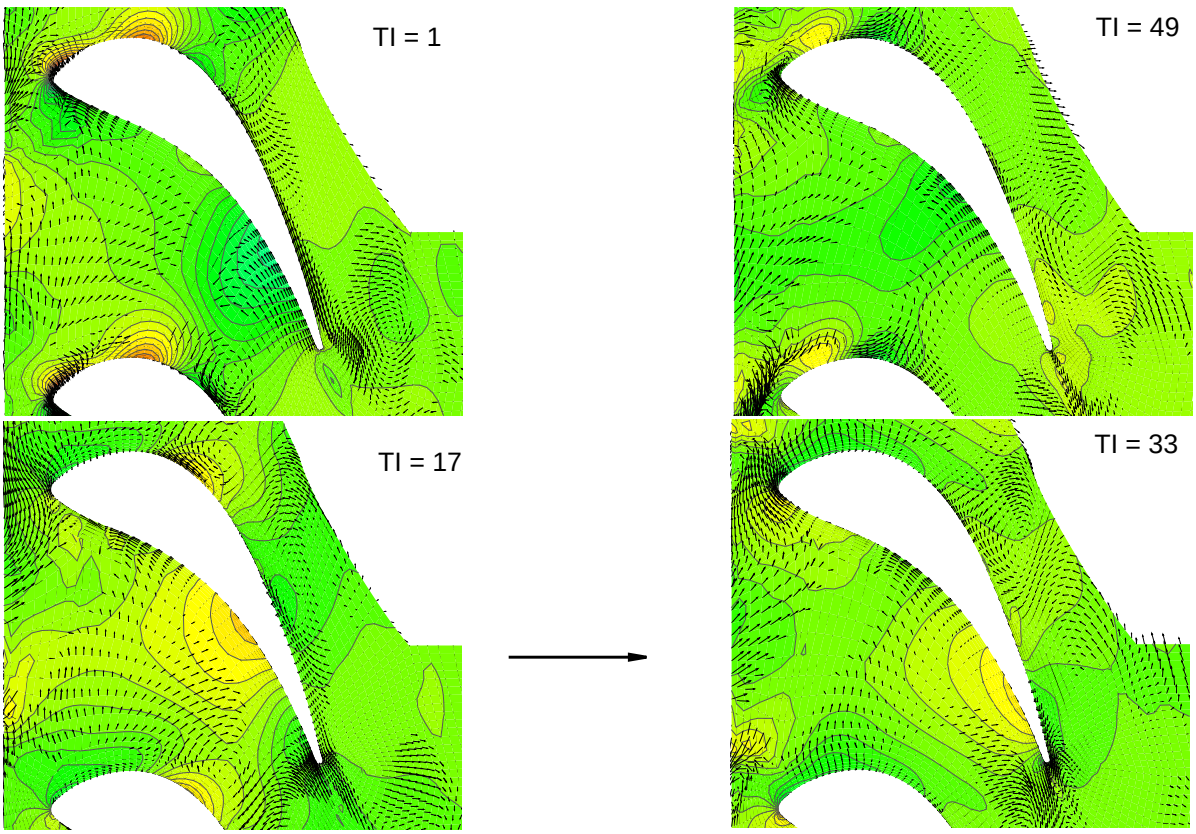

Fig. 11 Predicted instantaneous distribution of unsteady pressure contours and unsteady velocity vectors at stator 2, 96% span

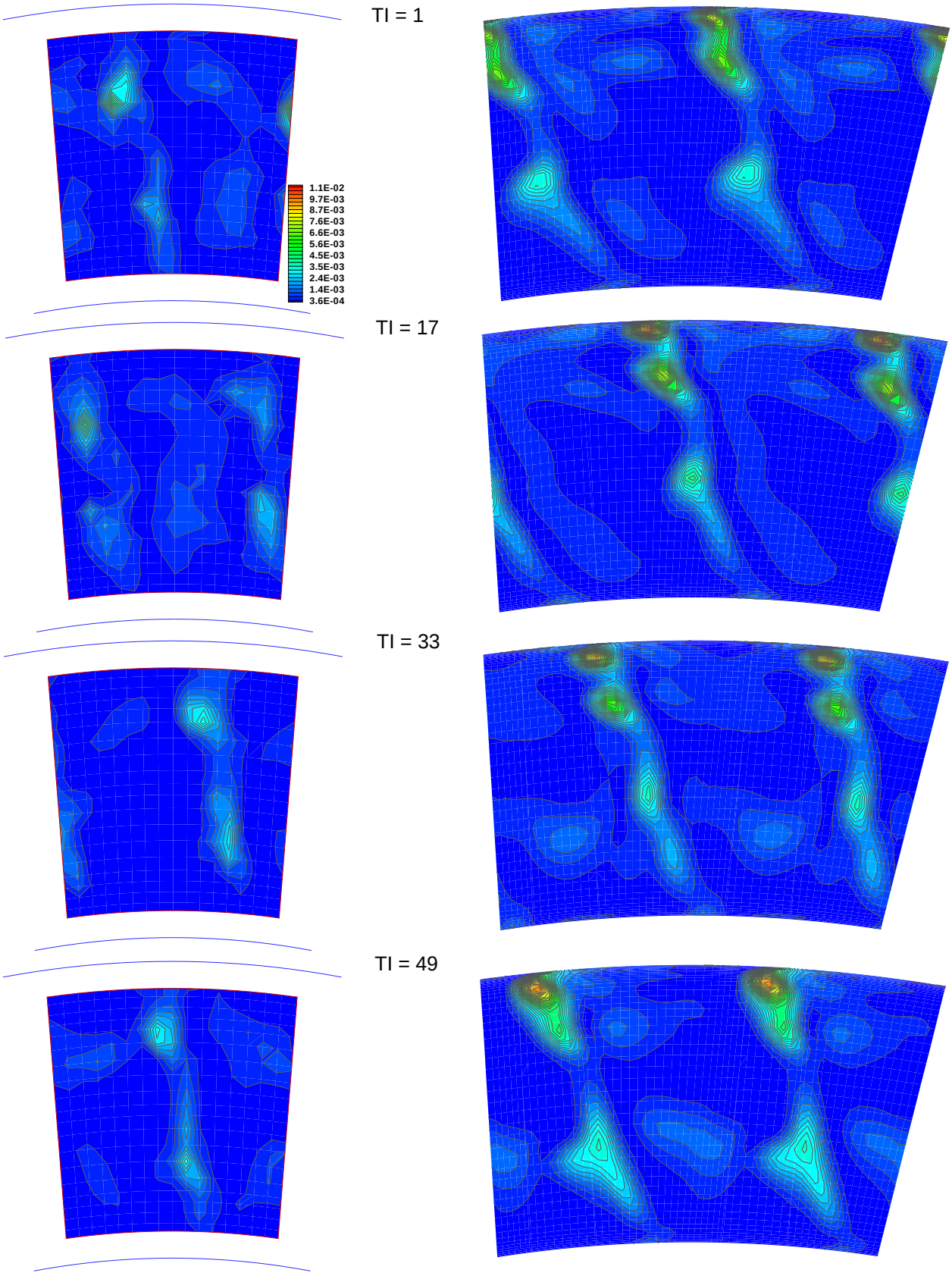

Fig. 12 Instantaneous distribution of unsteady kinetic energy at axial plane 2

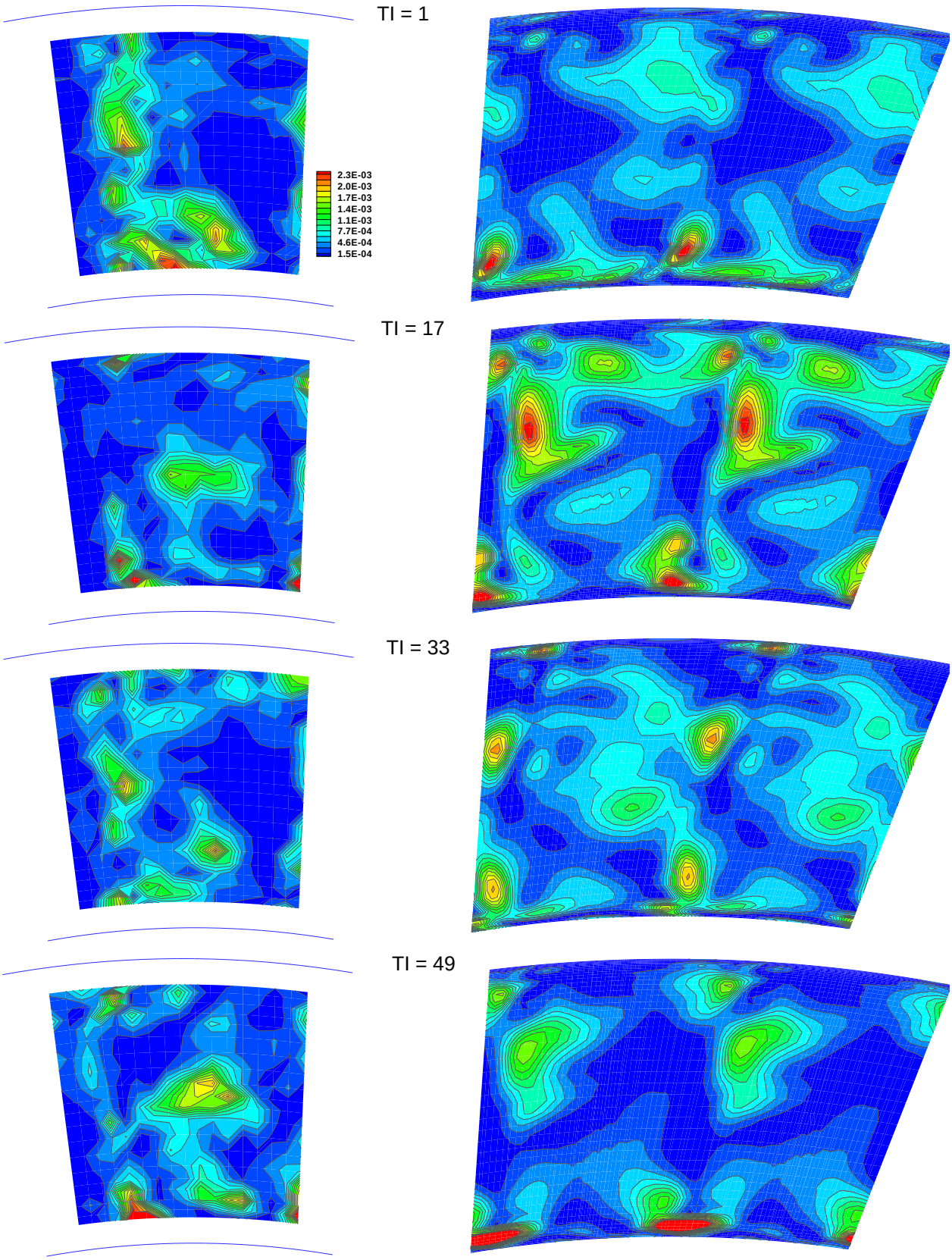

Fig. 13 Instantaneous distribution of unsteady kinetic energy at axial plane 3

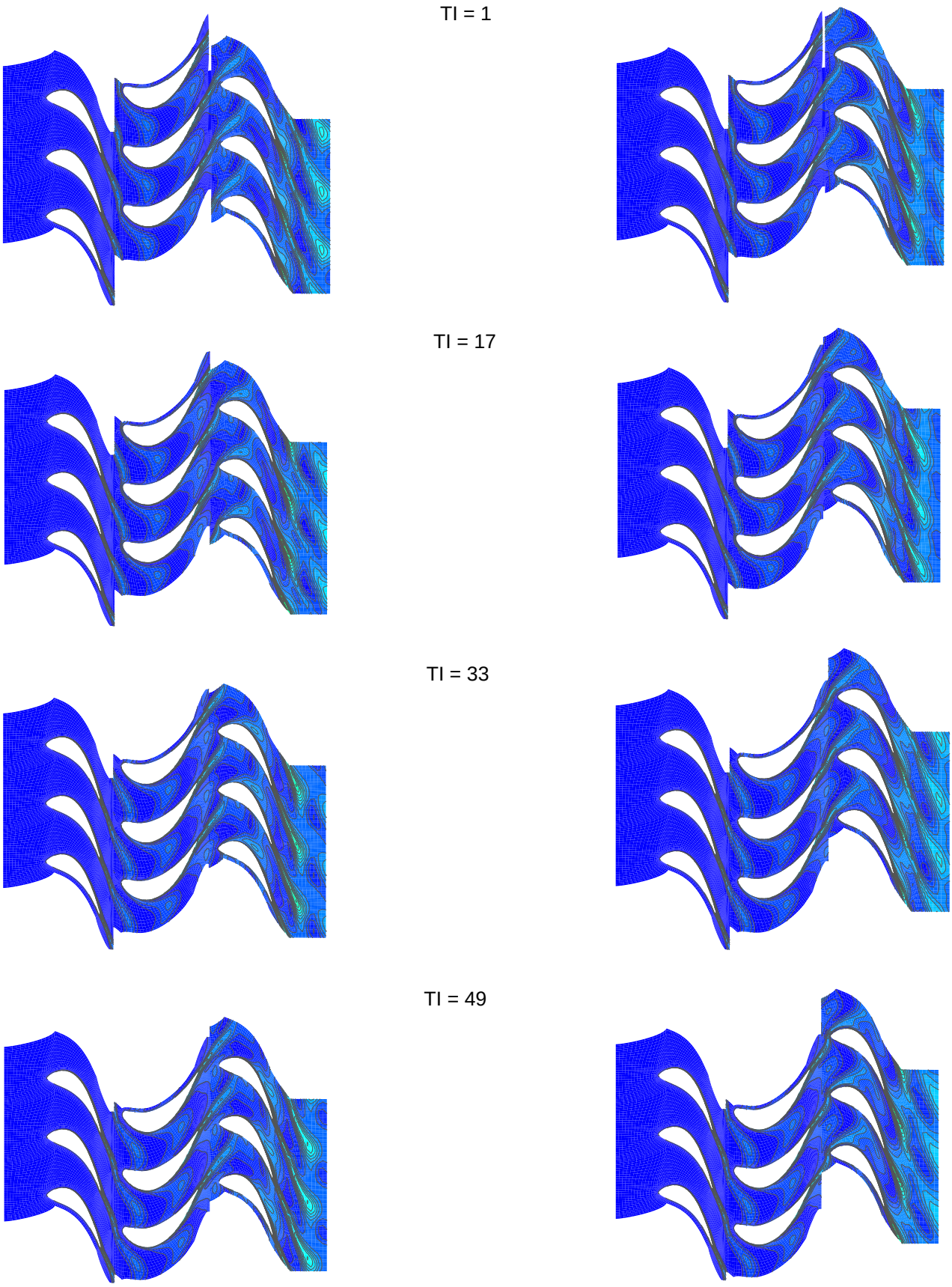

clocking angle: 2 (deg.) clocking angle: 6 (deg.)

Fig. 14 Instantaneous distribution of entropy at midspan during one rotor passing period

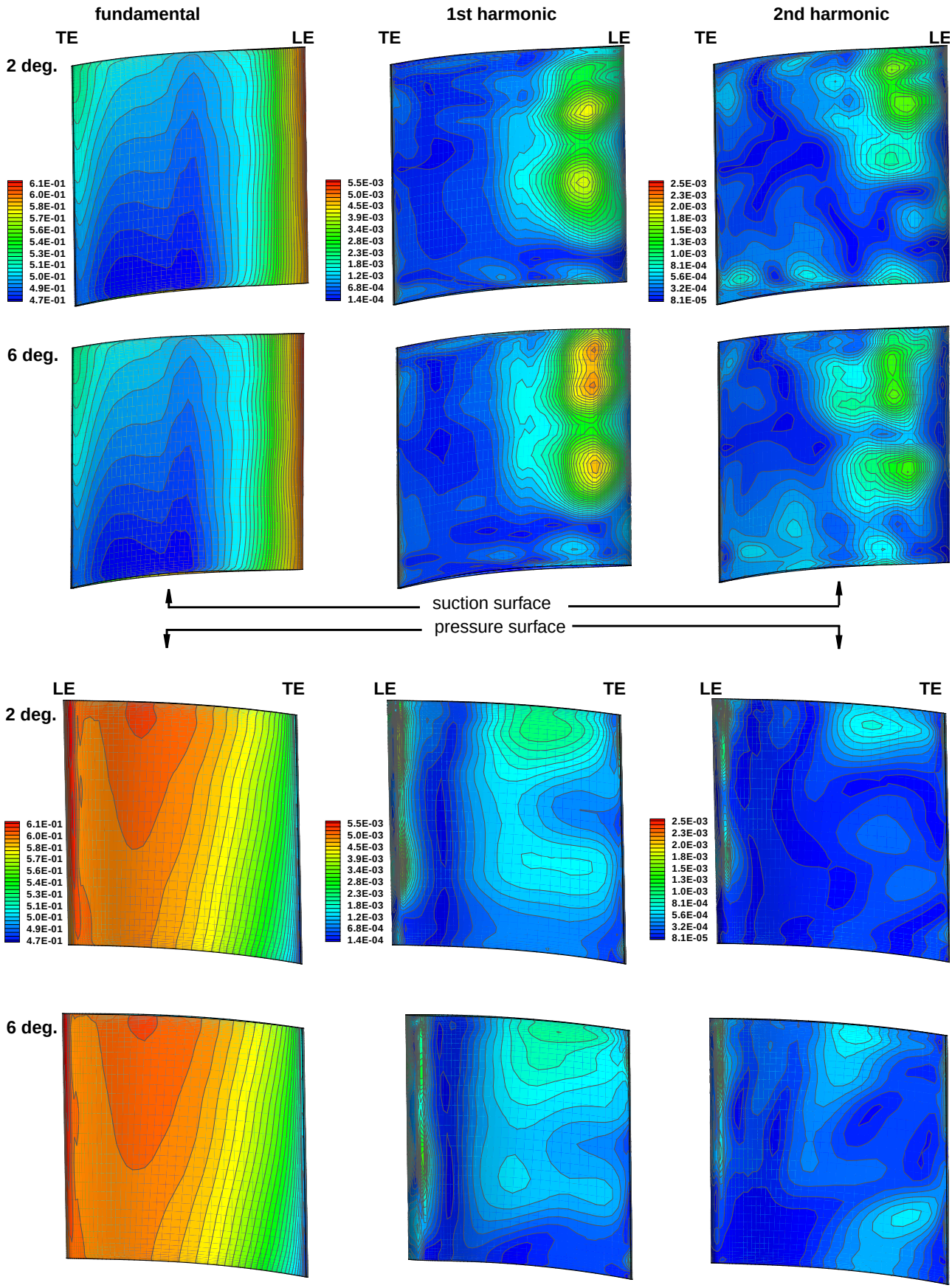

Fig. 15 Stator 2 blade computed fundamental, 1st and 2nd harmonics of pressure for clocking angles of 2 (deg.) and 6 (deg.)